Revision #2

Tracking the thermal decomposition of plasma-sprayed hydroxylapatite

Robert B. Heimann
Am Stadtpark 2A, D-02826 Görlitz, Germany

Abstract

In modern orthopedics, plasma-sprayed hydroxylapatite coatings are applied routinely to metallic parts of hip and knee prostheses, as well as to dental root implants in order to render them osseoconductive, that is, able to assist the body in creating new bone by ingrowth of bone cells, blood capillaries, and soft tissue. In this work, hydroxylapatite coatings were deposited by atmospheric plasma spraying on titanium alloy substrates, and characterized by synchrotron radiation X-ray diffraction and solid-state nuclear magnetic resonance spectroscopy. The deposition parameters were varied using a statistical design of experiments methodology. Depending on the degree of heat input and heat transfer rates, (i) dehydroxylated hydroxylapatite phases such as oxy- and oxyhydroxylapatite, (ii) thermal decomposition phases (tri- and tetracalcium phosphates, CaO), and (iii) amorphous calcium phosphate were formed. Implications of this research are that oxyapatite appears to be unstable at ambient conditions, and that proper selection of intrinsic plasma-spray parameters is key to the chemical stability and mechanical performance of the coating.

Keywords: Hydroxylapatite, oxyhydroxylapatite, oxyapatite, amorphous calcium phosphate, plasma spraying, osseoconductive coatings, implants.

Introduction

The apatite group of minerals with about 60 members crystallizing in the hexagonal space group $P6_3/m$ constitutes a scientifically and technologically important object of mineralogical research ever since the father of mineralogy, Abraham Gottlob Werner, described and named this mineral (Werner 1788). Calcium apatite serves mankind as an important source of fertilizer (Childers et al. 2011), carriers of rare earth elements (Pålsson et al. 2014), potential host material for nuclear (Vance and Gregg 2012) and non-nuclear (Pöllmann 2012) industrial wastes, and increasingly, as a biomedical material for filling bone cavities (Jarcho et al. 1976; Jarcho 1981), for bone (Pina and Ferreira 2012) and dental (Moseke and Gburek 2012) cements, as well as coatings for endoprosthetic implants (Ducheyne et al. 1980). It is this last application that is the subject matter of the present contribution.

To improve the biological performance of endoprosthetic, non-cemented hip and knee as well as dental implants, calcium phosphate bioceramic coatings have been developed as a bone growth-supporting interface between the load-carrying metal implant and the surrounding cortical bone tissue (Heimann and Lehmann 2015). Hydroxylapatite-derived implant coatings are known to be highly biocompatible as the bones of vertebrates, including humans, consist of a composite structure of oriented, nano-sized, non-stoichiometric hydroxylapatite crystallites intergrown with triple-helical collagen I microfibrils. Porous coatings allow the unimpeded ingrowth of bone cells, encouraging progressive vascularization, thereby anchoring the implant solidly within the cortical bone bed. Currently, plasma spraying of tens to hundreds of micrometer-sized hydroxylapatite particles is the most popular and the only Food and Drug Administration-approved method to coat implant surfaces for clinical application (Campbell 2003). However, there are serious shortcomings to this particular technique as the high temperature of the plasma jet causes the partial

dehydroxylation of hydroxylapatite to oxyhydroxylapatite and/or oxyapatite. This leads to subsequent, thermal decomposition by incongruent melting of the oxyapatite to form tricalcium phosphate ($Ca_3(PO_4)_2$, TCP) and tetracalcium phosphate ($Ca_4O(PO_4)_2$, TTCP) or even calcium oxide (CaO) by progressive evaporation of phosphorus pentoxide (see for example, Graßmann and Heimann 2000; Carayon and Lacout 2003). In addition, a thin layer of amorphous calcium phosphate forms preferentially at the interface of the plasma-sprayed coating to the metal substrate due to the rapid quenching of the molten impinging droplets, for which the heat transfer rates exceed 10^6 K/s (Heimann and Wirth 2006). During subsequent work it became clear that oxyapatite was considered by some researchers as the holy grail of implantology. Despite the diligent search for oxyapatite, its documentation has proven to be elusive up to the present day. In this contribution, the complex influence of the conditions of the plasma-spray application on the phase composition of hydroxylapatite coatings will be traced with particular reference to oxyapatite and amorphous calcium phosphate, key compounds that indicate the pathway of thermal decomposition of the initial hydroxylapatite feed material.

Materials and Methods

Principle of plasma spraying

Plasma spraying is a rapid solidification technology that requires a device to create a high-temperature jet of ionized argon or nitrogen gas in the form of a plasma. Such a device is called a plasmatron (plasma generator), which is powered by an electric arc or a high-frequency discharge. The surrounding atmosphere defines the type of plasma spraying device. If the surrounding medium is air, one speaks of air or atmospheric plasma spraying. Metal, ceramic, or even polymer powders or suspensions are injected by a stream of gas into the plasma, melted during the very short residence time in the jet, and propelled by the magneto-hydrodynamic

Lorentz force toward a target where the molten droplets solidify and build up a solid coating splat by splat. Any material can be sprayed as long as it has a well defined melting point, and does not decompose or sublimate during melting.

However, in practice many limitations persist. These include high coating porosity, insufficient adhesion to the substrate, occurrence of residual coating stresses, and line-of-sight technology (Heimann 2008). Despite its shortcomings, this technology has been largely adopted by industry as a rapid, well-controllable, and economic way to coat surfaces to impart advantageous functional properties including biological compatibility with living tissue. Although hydroxylapatite melts incongruently and thus partly decomposes in the hot plasma jet, plasma spray technology is still the method of choice to deposit bioactive calcium phosphate coatings on orthopedically approved metal surfaces.

Coating deposition

Calcium phosphate layers are deposited by atmospheric plasma spraying onto 50 x 10 x 2 mm^3 substrates, which consist of Ti alloyed with 6 at% Al and 4 at% V (Ti6Al4V). This alloy provides sufficient mechanical strength and corrosion resistance to withstand the deleterious action of the human body environment. Since it behaves in a bioinert way, it does not negatively interact with body tissue. The calcium phosphate layer imparts a bioactive, that is, a bone growth-supporting function to the otherwise bioinert metal surface.

Prior to spraying, the metal substrates are roughened by alumina grit and ultrasonically cleaned. The input feed of phase-pure hydroxylapatite powder (mean particle diameter: 120 µm) is manufactured via spray drying by Tomita Pharmaceutical, Japan. Three plasma-spraying parameters are selected that are known to influence significantly the heat input into the resultant coatings. These include traverse speed of the plasmatron, plasma gas

composition, and plasma power (Heimann 2008). A statistical design for experiments methodology was employed in which the three parameters are varied on two levels to yield a full-factorial 2^3 design of resolution IV. The design levels are as follows: traverse speed 150 and 500 mm/s; plasma gas composition (48.75 standard liters per minute (slpm) Ar + 1.25 slpm H_2 and 47.5 slpm Ar + 2.5 slpm H_2); and plasma power 11 and 24 kW (Table 1).

Coating deposition was carried out at Ecole Nationale Supérieure de Chimie de Lille (ENSCL) using a Praxair installation including a SG 100 plasmatron with internal powder injection. Parameters kept constant were the total plasma gas flow rate at 50 slpm; carrier gas (argon) flow rate at 3 slpm; powder feed rate at 18 g/min; and spray distance at 100 mm. The number of passes of the plasma jet across the substrate surface was adjusted to between 1 (at 500 mm/s traverse speed) and 3 (at 150 mm/s traverse speed) to yield an average coating thickness of 100 µm. The spray protocol was consistent with the procedure routinely applied at ENSCL (for example, Dyshlovenko et al. 2006).

Coating characterization

The plasma-sprayed coatings were investigated by high-resolution X-ray diffraction in conjunction with Rietveld refinement using synchrotron radiation at the ANKA Synchrotron Radiation Facility, Karlsruhe Institute of Technology (KIT)**.** The samples were irradiated on the PDIFF beamline in a 4-circle powder diffractometer equipped with a high-resolution detector for rapid data acquisition. The diffractometer was used in Bragg-Brentano geometry in conjunction with a Si(111) double-crystal monochromator.

^{1}H- and ^{31}P-CP-MAS (cross-polarization magic-angle spinning) NMR spectra were acquired on a BRUKER AVANCE 600 spectrometer operating at 14.1 T (Lamor frequency of 600.13 MHz) with a 4-mm probe. The experimental protocol was consistent with the parameters and procedure reported by Hartmann et al. (2001).

Results

Thermal dehydroxylation and decomposition of hydroxylapatite during plasma spraying is known to occur in four consecutive steps (Heimann 2006, 2012). Table 2 lists the reactions that occur in each step.

Using a technique that restricts the chemical changes in the hydroxyapatite feed to the first two dehydroxylation stages may appear to be a convenient way to retain basic structural elements of hydroxylapatite in oxyhydroxylapatite and/or oxyapatite. These (partially) dehydroxylated compounds indeed easily convert back to hydroxylapatite in the presence of moisture (cf. reverse of step 1 and step 2 reactions in Table 2) according to $O^{2-}(s) + \square(s) + H_2O(g) \rightarrow 2OH^-$ (Montel et al. 1980; Park et al. 2002). However, complete melting during plasma spraying is required to produce bioceramic coatings that possess properties of porosity, cohesive coating strength, and adhesion to the substrate that are conducive to biomedical applications. Despite many attempts, persistant problems arising from these two contradictory requirements remain to be solved.

Coating morphology

Figure 1 shows SEM micrographs of coating surfaces plasma-sprayed at low (sample #3) and high plasma powers (sample #6). Clearly, plasma power of 11 kW is insufficient to generate a well-molten and effectively spread-out coating. Instead, clusters of coarse-grained and very porous sintered agglomerates were formed attesting to only partial melting of the hydroxylapatite precursor particles (Fig. 1A). In contrast to this, application of plasma power of 24 kW resulted in a continuous and relatively smooth coating with low porosity (Fig. 1B). The limited heat input during spraying with 11 kW was thought to retain partly or fully dehydroxylated hydroxylapatite, a minimum of thermal decomposition phases (Table 2, steps 1 and 2) and, in particular, low amounts of amorphous calcium phosphate. However, in

clinical applications as an osseoconductive coating for implants, a structure like that in Figure 1A will not suffice, as its low coating cohesion and inadequate adhesion to the metallic substrate may lead to early failure by chipping, spalling, and, finally, delamination. In addition, hydroxylapatite particles only loosely attached to the coating surface may become liberated and transported by the lymphatic system to trigger hepatic cell degeneration. Moreover, risk analyses indicate that hydroxylapatite particles are involved in the so-called 'particle disease' (giant cell aggressive granulomatosis), leading to aseptic periprosthetic osteolysis, that is, mechanical failure of the prosthesis-bone interface arising primarily as the final result of bone loss occurring at this interface due to inflammation (Beck et al. 2012).

Synchrotron radiation X-ray diffraction

Lattice structural determination is required to document the phases produced farther into the thermal decomposition sequence. Whereas coatings deposited with higher heat transfer rates still retain a considerable amount of dehydroxylated hydroxylapatite phases such as 'oxyapatite', thermal decomposition products have already formed by step 3 (Table 2), such as ß-tricalcium phosphate. In addition, noticeable amounts of amorphous calcium phosphate occur, as shown by the strongly elevated background between about 27 and 37° 2Θ with a centroid value around 32° 2Θ (Fig. 2). This value ought to be compared to the values of the strongest interplanar spacings (211) of oxyapatite (Kay et al. 1964; Alberius-Henning et al. 1999) at 31.740(3)° 2Θ and of hydroxylapatite (Tas 2001) at 31.787(0)° 2Θ.

Figure 3 compares the synchrotron radiation X-ray diffraction pattern (CuKα) at low diffraction angles for coatings deposited with low (trace A, sample #3) and high (trace B, sample #6) plasma power. Higher plasma power translates to higher heat input into the hydroxylapatite powder as a large part of the electrical energy spent on ionization of the plasma gas will be recovered by recombination in the form of heat. This increased heat input leads to increased dehydroxylation of hydroxylapatite: whereas coatings deposited at low

plasma power display a 'clean' dehydroxylated hydroxylapatite (oxy- and/or oxyhydroxylapatite) pattern. Spraying with higher power reveals the thermal decomposition products ß-tricalcium and tetracalcium phosphate (Table 2, step 3) formed by incongruent melting of oxyapatite and, in particular, CaO (Table 2, steps 4a and b) indicating evaporative loss of P_2O_5 from calcium phosphates.

Amorphous calcium phosphate vs. oxy- and oxyhydroxylapatite

Those hydroxylapatite particles that are fully melted during plasma spraying will solidify during cooling on the substrate surface. The nature of the resulting phases therefore depends on the cooling rate. As nucleation is impeded during rapid quenching, high cooling rates produce amorphous calcium phosphate. Despite the high temperature encountered during plasma spraying, amorphous calcium phosphate still contains substantial amounts of protons and OH^- ions as revealed by electron energy loss spectroscopy (EELS; Heimann and Wirth 2006). These residual ions are thought to act as a driving force for the (partial) crystallization of amorphous calcium phosphate to hydroxylapatite during cooling (Gross et al. 1998d). Quantitative determination of the amount of amorphous calcium phosphate by the Keller-Dollase method (Keller and Dollase 2000) revealed that increasing the plasma power increased the amount of amorphous calcium phosphate formed (Fig. 4). The method uses a non-linear least-squares fitting of the non-crystalline X-ray scattering maximum around 32° 2Θ from which an 'index of crystallinity' is derived as a figure of merit. By this method, sample #3 deposited at low heat input showed about 25 mass% amorphous calcium phosphate (Fig. 5A), whereas sample #6 deposited at high heat input showed 40 mass% amorphous calcium phosphate (Fig. 5B).

In contrast to the above, reduced cooling rates, instead of producing only amorphous calcium phosphate, may lead to retention in the coating of oxy- and/or oxyhydroxylapatite.

This effect is experienced particularly at the topmost coating layer or in splats deposited onto previously sprayed, already cooled calcium phosphates with low thermal diffusivity (Gross and Pluduma 2012). Unfortunately, the unequivocal detection of oxyapatite by conventional X-ray diffraction techniques is considered problematic (Gross et al. 1998a; Gross and Berndt 1998b), since the c-axis dimension of oxyapatite is only marginally larger than that of hydroxylapatite (Trombe 1973; Montel et al. 1980). This fact accounts for only a very small shift of the (002) interplanar spacing to smaller diffraction angles (Gross et al. 1998c). The subtle lattice expansion during dehydroxylation of hydroxylapatite is presumably caused by the larger Shannon crystal radius of the O^{2-} ion (135 pm) compared to that of the OH^- ion (118 pm). Hence, very accurate measurements are required, for example, high-resolution X-ray powder diffraction by synchrotron radiation. Such measurements were performed on plasma-sprayed hydroxylapatite coatings using the ANKA Synchrotron Radiation Facility at the Karlsruhe Institute of Technology (KIT).

Evidently, under ambient conditions, oxyapatite is metastable at best. Indeed, Trombe and Montel (1978) demonstrated the only condition of oxyapatite stability to be under vacuum or in sufficiently water-free gas atmospheres at 850–1050°C. This oxyapatite was found to be highly reactive at temperatures below 800°C and to undergo, even under vacuum, rehydroxylation to oxyhydroxylapatite, which was stable in air to ambient temperature. The strong tendency of dehydroxylated hydroxylapatite to restore OH ions was confirmed by FTIR spectroscopy, thermal analyses (TGA, DTA), and mass spectrometry by Park et al. (2002). In contrast, at temperatures above 1050 °C, oxyapatite decomposes to a mixture of tricalcium- and tetracalcium phosphates (Step 3, Table 2).

Nuclear magnetic resonance spectroscopy

Additional salient information on the phase content of plasma-sprayed hydroxylapatite has been gained from nuclear magnetic resonance spectroscopy. Figure 5 shows cross-polarized (CP) magic angle spining (MAS) nuclear magnetic resonance (NMR) spectra of protons (Fig. 5A) and PO_4^{3-} tetrahedral groups (Fig. 5B) of typical plasma-sprayed hydroxylapatite coatings. The suggested assigments of individual bands are tentative (Table 3), based on earlier work by Hartmann et al. (2000, 2001) and the author (Heimann et al. 2003). The isotropically shifted L* band of the ^{1}H-NMR spectrum, shown in Fig. 5A, may be a (weak) indication of the existence of oxy- and/or oxyhydroxylapatite-like conformations. More profitable is the ^{31}P-NMR spectrum. Besides the A signal of well-ordered and highly crystalline hydroxylapatite, apparently unchanged from its original composition, there are C and D signals that are thought to be related to PO_4^{3-} groups with strongly to very strongly distorted environments and few or no associated OH^- groups, typical for oxyhydroxylapatite and oxyapatite. The B signal is thought to be associated with strongly distorted PO_4^{3-} tetrahedral groups without neighboring OH^- groups, indicating the presence of tri- and tetracalcium phosphate.

Additional 2D-double quantum, ^{1}H/^{31}P cross-polarization, heteronuclear correlation (HETCOR) NMR spectroscopy (not shown here) confirmed that the D band is indeed related to oxyapatite as already proposed by Hartmann et al. (2000). Since this chemical shift is identical to that of tetracalcium phosphate, it can be concluded that with increasing dehydroxylation of hydroxylapatite the coating composition eventually approaches that of structurally closely related tetracalcium phosphate (Mathew and Takagi 2001), in accord with the dehydroxylation succession HAp → O-HAp → OAp → TTCP shown in Table 2. Tetracalcium phosphate, $Ca_4O(PO_4)_2$ crystallizes in the monclinic space group $P2_1$ whereby the Ca^{2+} and PO_4^{3-} ions are located in four sheets perpendicular to the b axis. As each sheet contains two Ca-P columns and one Ca-Ca column, a structure similar to glaserite, $K_3Na(SO_4)_2$ with surplus oxygen ions results (Dickens et al. 1973; Mathew and Takagi 2001).

Two adjacent sheets form a double layer closely related to the structure of hydroxylapatite. This similarity is the root of re-formation of hydroxylapatite during reaction of tetracalcium phosphate with HPO_4^{2-} moieties in dental self-setting bone cement according to

$$2\ Ca_4O(PO_4)_2 + 2\ Ca^{2+} + 2\ HPO_4^{2-} \rightarrow Ca_{10}(PO_4)_6(OH)_2. \quad (1)$$

Discussion

The oxyapatite, $Ca_{10}(PO_4)_6O$, question has a long and colorful but highly controversial history. Oxyapatite as a stable mineral was first proposed by J.A. Voelcker (1883) in his doctoral dissertation, and this compound was subsequently named voelckerite by Rogers (1912, 1914).

However, the existence of pure oxyapatite stable at ambient conditions was already questioned by Bredig et al. (1933) who drafted one of the earliest CaO-P_2O_5 phase diagrams in the absence of water. Instead, they proposed the existence of 'mixed' apatites, that is, oxyhydroxylapatites $Ca_{10}(PO_4)_6X_{2-2n}O_n$ (X = OH, F; $0 < n < 1$) based on experimental evidence. They also concluded that the X (c-axis channel) position could not be left empty. In particular, no superstructures were found by X-ray analysis that would point to an ordered distribution of O^{2-} ions in the c-axis channel. It ought to be mentioned that such ordering would require a doubling of the c-axis length in order to sustain ordered occupancy of only half of the A-sites ± (0,0,1/4) or B-sites ± (0,0,1/2) (Merker and Wondratschek 1960; Merker et al. 1970). Subsequently, the existence of OH- and halogen-deficient apatites was confirmed by McConnell and Hey (1969).

In support of the assumption of the non-existence of stable oxyapatite, a computational investigation (De Leeuw et al. 2007) confirmed that formation of oxygen vacancies in the c-axis channels of hydroxylapatite is thermodynamically unfavourable. Despite these

thermodynamic constraints, investigations by Alberius-Henning et al. (1999) into the structure of oxyapatite suggested that there exists a linear chain of O^{2-} ions parallel to the c-axis, each one followed by a vacancy. Calderin et al. (2003) performed modelling by density-functional theory with local-density approximation (DFT-LDA) and first-principles pseudo-potentials. These authors conjectured that variations of the total densities of Kohn-Sham states (DOS) may provide a means to differentiate between hydroxylapatite and oxyapatite, since in the energy gaps of oxyapatite several states are present that are absent in hydroxylapatite. The defect apatite structure appears to be insensitive to the choice of the anion (OH^-, F^-, Cl^-, O^{2-}, □) in the c-axis column. If these anions are removed completely by heating, the structure remains largely unchanged and at least metastable. Indeed, investigations by Liao et al. (1999) showed that even after a loss as high as 75% of the OH group in the c-axis channel, the apatite structure will be maintained. However, complete loss of OH was never observed, that is, a small amount of OH is always present in the oxyapatite structure. The limiting composition is then $Ca_{10}(PO_4)_6(OH)_{0.5}O_{0.75}$ (n = ¾), which corresponds to an experimentally observed water loss of 1.34 mass% and accounts for the released OH^- (Trombe and Montel 1971).

Implications

The investigation of the existence of metastable oxyapatite and amorphous calcium phosphate in plasma-sprayed bioceramic implant coatings constitutes an important precondition to understanding the pathways conducive to the formation of bone-like, that is, Ca-deficient secondary hydroxylapatite during restoration of the apatite structure *in vivo*. The presence and the varying amounts of oxyapatite and/or oxyhydroxylapatite affect the dissolution behavior and the recrystallization kinetics of bioceramic coatings as well as their mechanical performance in orthopedic and dental applications. Hence, knowledge of the conditions under which oxyapatite may occur in plasma-sprayed hydroxylapatite coatings, and its

304 transformation to secondary, bone-like apatite is of high interest when designing and applying
305 such coatings with superior biomedical performance in a clinical environment.

306 The continuous amorphous calcium phosphate layer formed at high quenching rates
307 adjacent to the coating-substrate interface will dissolve preferentially during interaction with
308 body fluid. The compromised amorphous calcium phosphate layer thereby provides a least-
309 energy fracture path for coating separation and thus is one of the leading causes of coating
310 delamination *in vivo* (Park and Condrate 1999). Dissolution of the amorphous calcium
311 phosphate layer will be accelerated when cracks form perpendicular to the coating surface as
312 the result of relief of residual stresses. Such cracks will channel biofluid down to the
313 amorphous calcium phosphate layer. Hence, investigation of crack formation goes a long way
314 toward inhibiting and controlling the dissolution of amorphous calcium phosphate *in vivo*.

315 The degree of dehydroxylation and decomposition of hydroxylapatite during
316 atmospheric plasma spaying depends on heat input and heat transfer rates, respectively.
317 Doubling the plasma power from 11 to 24 kW leads to an increase of the amount of
318 amorphous calcium phosphate from 25 to 40 mass%. Whereas plasma power of only 11 kW
319 results in exclusive formation of partially dehydroxylated hydroxylapatite
320 (oxyhydroxylapatite), plasma power of 24 kW causes thermal decomposition towards tri- and
321 tetracalcium phosphates as well as CaO. In particular, the latter is deleterious to the biological
322 performance of hydroxylapatite coatings as it is known to drive up the local pH, which causes
323 cytotoxic effects on living bone cells (Le Geros et al. 1991; Chou et al. 1999).

324 Solid-state NMR spectroscopy permits the specification of the structural environments of
325 protons and tetrahedral PO_4^{3-} moieties, whereby strongly distorted tetrahedra point to the co-
326 existence of oxyhydroxylapatite and metastable oxyapatite. The latter transfers through
327 incongruent melting to tri- and tetracalcium phosphates. Owing to the high solubility of the
328 decomposition phases as well as amorphous calcium phosphate under physiological

329 conditions, stringent control of the decomposition sequence by proper selection of intrinsic
330 plasma spray parameters is mandatory to ensure satisfactory implant performance.

331 **Acknowledgements**

332 The author is much indebted to Lech Pawlowski, now at Université de Limoges, France for
333 providing the plasma-sprayed coatings, to Horst J. Pentinghaus, Dettenheim, Germany for
334 arranging the X-ray diffraction studies at KIT, and to Peter Hartmann, Westsächsische
335 Hochschule Zwickau, Germany for assistance with the NMR work. Jill D. Pasteris,
336 Washington University, St. Louis, Missouri, USA is acknowledged for competently and
337 thoroughly reviewing the manuscript.

338 **References**

339 Alberius-Henning, P., Landa-Canovas, A., Larsson, A.K., and Lidin, S. (1999) Elucidation of
340 the crystal structure of oxyapatite by high-resolution electron microscopy. Acta
341 Crystallographica, B55, 170-176.

342 Beck, R.T., Illingworth, K.D., and Saleh, K.J. (2012) Review of periprosthetic osteolysis in
343 total joint arthroplasty: an emphasis on host factors and future directions. Journal of
344 Orthopaedic Research, 30(4), 541-546.

345 Bredig, M.A., Franck, H.H., und Füldner, H. (1933) Beiträge zur Kenntnis der Kalk-
346 Phosphorsäure-Verbindungen II. Zeitschrift für Elektrochemie, 39(12), 959-969.

347 Calderin, L., Stott, M.J., and Rubio, A. (2003) Electronic and crystallographic structure of
348 apatite. Physical Review, B67, 134106-12.

349 Campbell, A.A. (2003) Bioceramic for implant coatings. Materialstoday, November, 26-30.

350 Carayon, M.T., and Lacout, J.L. (2003) Study of the Ca/P atomic ratio of the amorphous
351 phase in plasma-sprayed hydroxyapatite coatings. Journal of Solid State Chemistry, 172, 339-
352 350.

353 Childers, D. L., Corman, J., Edwards, M., and Elser, J. J. (2011) Sustainability challenges of
354 phosphorus and food: solutions from closing the human phosphorus cycle. Bioscience, 61,
355 117–124.

356 Chou, L., Marek, B., and Wagner, W.R. (1999) Effect of hydroxyapatite coating crystallinity
357 on biosolubility, cell attachment efficiency, and proliferation in vitro. Biomaterials, 19, 977-
358 985.

359 De Leeuw, N., Bowe, J.R., and Rabone, J.A.L. (2007) A computational investigation of
360 stoichiometric and calcium-deficient oxy- and hydroxyapatite. Faraday Discussions, 134, 195-
361 214.

Dickens, B., Brown, W.E., Kruger, G.J., and Steward, J.M. (1973) $Ca_4(PO_4)_2O$, tetracalcium diphosphate monoxide. Crystal structure and relationship to $Ca_5(PO4)_3OH$ and $K_3Na(SO_4)_2$. Acta Crystallographica, B29, 2046-2056.

Ducheyne, P., Hench, L.L., Kagan, I.I., Martens, A., Bursens, A., and Mulier, J.C. (1980) Effect of hydroxyapatite impregnation on skeletal bonding of porous coated implants. Journal of Biomedical Materials Research, 14, 225-237.

Dyshlovenko, S., Pawlowski, L., Roussel, P., Murano, D., and La Maguer, A. (2006) Relationship between plasma spray operational parameters and microstructure of hydroxyapatite coatings and powder particles sprayed into water. Surface & Coating Technology, 200, 3845-3855.

Graßmann, O., and Heimann, R.B. (2000) Compositional and microstructural changes of engineered plasma-sprayed hydroxyapatite coatings on Ti6Al4V substrates during incubation in protein-free simulated body fluid. Journal of Biomedical Materials Research, 53(6), 685-693.

Gross, K.A., and Berndt, C.C. (1998b) Thermal processing of hydroxyapatite for coating production. Journal of Biomedical Materials Research, 39, 580-587.

Gross, K.A., and Pluduma, L. (2012) Putting oxyhydroxyapatite into perspective: a pathway to oxyapatite and its applications. In R.B. Heimann, Ed., Calcium Phosphate: Structure, Synthesis, Properties, and Applications, p. 95-120. Biochemistry Research Trends. Nova Science Publishers, Inc., New York.

Gross, K.A., Berndt, C.C., and Herman, H. (1998d) Amorphous phase formation in plasma-sprayed hydroxyapatite coatings. Journal of Biomedical Materials Research, 39, 407-414.

Gross, K.A., Berndt, C.C., Stephens, P., and Dinnebier, R. (1998c) Oxyapatite in hydroxyapatite coatings. Journal of Materials Science: Materials in Medicine, 33, 3985-3991.

Gross, K.A., Ben-Nissan, B., Walsh, W.R., and Swarts, E. (1998a) Analysis of retrieved hydroxyapatite coated orthopaedic implants. In C. Coddet, Ed., Thermal Spray. Meeting the Challenges of the 21st Century, p. 1133-1138. Proc. 15th ITSC, May 25-29, Nice, France.

Hartmann, P., Barth, S., Vogel, J., and Jäger, C. (2000) Investigations of structural changes in plasma-sprayed hydroxyapatite coatings. In D. Rammlmair, J. Mederer, Th. Oberthür, R.B. Heimann and H. Pentinghaus, Eds, Applied Mineralogy in Research, Economy, Technology, Ecology and Culture, vol. 1, p. 147-150. Proc. 6th ICAM 2000. A.A. Balkema, Rotterdam.

Hartmann, P., Jäger, C., Barth, S., Vogel, J., and Meyer, K. (2001) Solid state NMR, X-ray diffraction, and infrared characterization of local structure in heat-treated oxyhydroxyapatite microcrystals: an analog of the thermal decomposition of hydroxyapatite during plasma-spray procedure. Journal of Solid State Chemistry, 160(2), 460-468.

Heimann, R.B. (2006) Thermal spraying of biomaterials. Surface & Coating Technology, 201(5), 2012-2019.

Heimann, R.B. (2008) Plasma Spray Coating. Principles and Applications, 2nd ed., 427 pp. Wiley-VCH, Weinheim, Germany.

Heimann, R.B. (2012) Structure, properties, and biomedical performance of osteoconductive bioceramic coatings. Surface & Coating Technology, 233, 27-38.

Heimann, R.B. and Lehmann, H.D. (2015) Bioceramic Coatings for Medical Implants. Trends and Techniques, 467 pp. Wiley-VCH, Weinheim, Germany.

Heimann, R.B., and Wirth, R. (2006) Formation and transformation of amorphous calcium phosphate on titanium alloy surfaces during atmospheric plasma spraying and their subsequent in vitro performance. Biomaterials, 27, 823-831.

Heimann, R.B., Tran, H.V., and Hartmann, P. (2003) Laser-Raman and nuclear magnetic resonance (NMR) studies on plasma-sprayed hydroxyapatite coatings: influence of bioinert bond coats on phase composition and resorption kinetics in simulated body fluid. Materialwissenschaft und Werkstofftechnik, 34 (12), 1163-1169.

Jarcho, M. (1981) Calcium phosphate ceramics as hard tissue prosthetics. Clinical Orthopaedics and Related Research, 157, 259-278.

Jarcho, M., Bolen, C.H., Thomas, M.B., Bobick, J., Kay, J.F., and Doremus, R.H. (1976) Hydroxylapatite synthesis and characterization in dense polycrystalline form. Journal of Materials Science, 11, 2027-2035.

Kay, M.I., Young, R.A., and Posner, A.S. (1964) Crystal structure of hydroxyapatite. Nature (London), 204, 1050-1053.

Keller, L., and Dollase, W.A. (2000) X-ray determination of crystalline hydroxyapatite to amorphous calcium phosphate ratio in plasma sprayed coatings. Journal of Biomedical Materials Research, 49, 244-249.

Le Geros, R.Z., Orly, I., Gregoire, M., and Daculsi, G. (1991) Substrate surface dissolution and interfacial biological mineralization. In J.E. Davies, Ed., The Bone-Biomaterial Interface, p. 76-88. University of Toronto Press, Toronto.

Liao, C.J., Lin, F.H., Chen, K.S., and Sun, J.S. (1999) Thermal decomposition and reconstruction of hydroxyapatite in air atmosphere. Biomaterials, 20, 1807-1813.

Mathew, M., and Takagi, S. (2001) Structures of biological minerals in dental research. Journal of Research of the National Institute of Standards and Technology, 106(6), 1035-1044.

McConnell, D., and Hey, M.H. (1969) The oxyapatite (voelckerite) problem. Mineralogical Magazine, 37(86), 301-303.

Merker, L., und Wondratschek, H. (1960) Der Oxypyromorphit $Pb_{10}(PO_4)_6O$ und der Ausschnitt $Pb_4P_2O_5$-$Pb_3(PO_4)_2$ des Systems PbO-P_2O_5. Zeitschrift für Anorganische und Allgemeine Chemie, 306, 25-29.

Merker, L., Engel, G., Wondratschek, H., and Ito, J. (1970) Lead ions and empty halide sites in apatites. American Mineralogist, 55, 1435-1437.

Montel, G., Bonel, G., Trombe, J.C., Heughebaert, J.C., and Rey, C. (1980) Progress dans le domaine de la chimie des composes phosphores solides a structure d'apatite. Pure and Applied Chemistry, 52(4), 973-987.

Moseke, C., and Gburek, U. (2012) Tetracalcium phosphate-based dental cements. In R.B. Heimann, Ed., Calcium Phosphate: Structure, Synthesis, Properties, and Applications, p. 333-342. Biochemistry Research Trends. Nova Science Publishers, Inc., New York.

Pålsson, B.I., Martinsson, O., Wanhainen, C., and Frederiksson, A. (2014) Unlocking rare earth elements from European apatite-iron ores. Proceedings 1st European Rare Earth Resources Conference (ERES2014), p. 211-220, Milos, Greece.

Park, E., and Condrate, R.A. (1999) Graded coating of hydroxyapatite and titanium by atmospheric plasma spraying. Materials Letters, 40, 228-234.

Park, E., Condrate, R.A., Lee, D., Kociba, K., and Gallagher, P.K. (2002) Characterization of hydroxyapatite: before and after plasma spraying. Journal of Materials Sciences: Materials in Medicine, 13, 211-218.

Pina, S., and Ferreira, J.M.F. (2012) Calcium phosphate bone cement. In R.B. Heimann, Ed., Calcium Phosphate: Structure, Synthesis, Properties, and Applications, p. 303-332. Biochemistry Research Trends. Nova Science Publishers, Inc., New York.

Pöllmann, H (2012) The use of apatite-type minerals for immobilization purposes. In R.B. Heimann, Ed., Calcium Phosphate: Structure, Synthesis, Properties, and Applications, p. 409-443. Biochemistry Research Trends. Nova Science Publishers, Inc., New York.

Rogers, A.F. (1912) Dahlite (podolite) from Tonopah, Nevada; voelckerite, a new basic calcium phosphate; remarks on the chemical composition of apatite and phosphate rocks. American Journal of Science, 33, 475-482.

Rogers, A.F. (1914) A new locality for voelckerite and the validity of voelckerite as a mineral species. Mineralogical Magazine, 17, 155-162.

Tas, A.C. (2001) X-ray diffraction data for flux-grown calcium hydroxyapatite whiskers. Powder Diffraction, 16(2), 102-106.

Trombe, J.C. (1973) Contribution á l'étude de la decomposition et de la réactivité de certaines apatites hydroxylées et carbonates. Annales de Chimie (Paris), 14th ser., 8, 335-347.

Trombe, J.C., and Montel, G. (1971) Sur la préparation del'oxyapatite phospho-calcique. Comptes Rendus de l'Académie des Sciences Paris, 273, 462-465.

Trombe, J.C., and Montel, G. (1978) Some features of the incorporation of oxygen in different oxidation states in the apatite lattice. Journal of Inorganic and Nuclear Chemistry, 40, 15-21; 27-30.

Vance, E.R., and Gregg, D.J. (2012) Calcium phosphate materials for radioactive waste immobilisation. In R.B. Heimann, Ed., Calcium Phosphate: Structure, Synthesis, Properties, and Applications, p. 445-465. Biochemistry Research Trends. Nova Science Publishers, Inc., New York.

Voelcker, J.A. (1883) Die chemische Zusammensetzung des Apatits nach eigenen vollständigen Analysen. Berichte der Deutschen Chemischen Gesellschaft, 16, 2460-2464.

Werner, A.G. (1788) Geschichte, Karakteristik, und kurze chymische Untersuchung des Apatits. Bergmännisches Journal, 1, 76-96.

List of figure captions

Figure 1 Scanning electron micrographs of plasma-sprayed hydroxylapatite coatings. A: at low plasma power (sample # 3, Table 1). B: at high plasma power (sample # 6, Table 1).

Figure 2 Synchrotron radiation X-ray diffraction pattern (CuKα) of hydroxylapatite plasma-sprayed with plasma power of 24 kW, traverse speed of 500 mm/s, and plasma gas composition of 48.75 slpm Ar + 1.25 slpm H_2 (sample #6, Table 1) showing hydroxyl-deficient hydroxylapatite ('oxyapatite', XRPDF 89-649; 04-011-1880) and ß-tricalcium phosphate (asterisks, XRPDF 04-014-2292).

Figure 3 Synchrotron radiation X-ray diffraction pattern (CuKα) of hydroxylapatite coatings plasma-sprayed at 11 kW (trace A, sample #3, Table1) and 24 kW (trace B, sample #6, Table 1) plasma powers. The most obvious distinguishing criterion is the strong peak related to CaO from trace B.

Figure 4 Non-linear last-squares fitting to determine the amount of amorphous calcium phosphate. A: sample #3, Table 1. B: sample #6, Table 1.

Figure 5 CP-MAS-NMR spectra of an as-sprayed hydroxylapatite coating. A: ^{1}H-CP-MAS NMR spectrum. B: ^{31}P-CP-MAS NMR spectrum. The insets show the spectra of phase-pure stoichiometric hydroxylapatite as a reference. For explanation see text.

Table 1 Statistical design of experiments (SDE) matrix (Yates order). *standard liter per minute.

Sample #	Traverse speed (mm/s)	Plasma gas composition (slpm)*	Plasma power (kW)	Reference
1	150	48.75 Ar/1.25 H_2	11	
2	500	48.75 Ar/1.25 H_2	11	Figure 4
3	**150**	**47.5 Ar/2.5 H_2**	**11**	Figures 1A,3,4,5A
4	500	47.5 Ar/2.5 H_2	11	
5	150	48.75 Ar/1.25 H_2	24	
6	**500**	**48.75 Ar/1.25 H_2**	**24**	Figures 1B,2,3,4,5B
7	150	47.5 Ar/2.5 H_2	24	

8	500	47.5 Ar/2.5 H_2	24	

Table 2 Thermal decomposition sequence of hydroxylapatite (Carayon and Lacout 2003)

Step 1:	$Ca_{10}(PO_4)_6(OH)_2$ (hydroxyapatite)	→	$Ca_{10}(PO_4)_6(OH)_{2-2x}O_x\square_x + xH_2O$ (oxyhydroxyapatite)
Step 2:	$Ca_{10}(PO_4)_6(OH)_{2-2x}O_x\square_x$ (oxyhydroxyapatite)	→	$Ca_{10}(PO_4)_6O_x\square_x + (1-x)H_2O$ (oxyapatite)
Step 3:	$Ca_{10}(PO_4)_6O_x\square_x$ (oxyapatite)	→	$2Ca_3(PO_4)_2$ (tricalcium phosphate) + $Ca_4O(PO_4)_2$ (tetracalcium phosphate)
Step 4a:	$Ca_3(PO_4)_2$	→	$3\,CaO + P_2O_5$
Step 4b:	$Ca_4O(PO_4)_2$	→	$4CaO + P_2O_5$

Table 3 Assigment of NMR band shown in Fig. 5A and B. HAp hydroxylapatite, OAp oxyapatite, O-HAP oxyhydroxylapatite, TCP tricalcium phosphate, TTCP tetracalcium phosphate.

Band	**Band position (ppm)**		**Phase assignment**
^{1}H		**Structural assignment of protons**	
L	-0.1 ± 0.1	Protons in stoichiometric, highly crystalline hydroxylapatite	HAp
L*	-1.3 ± 0.3	Isotropically shifted protons in distorted SRO structures (oxy- or oxyhydroxylapatite)	OAp, O-HAp
G	+1.3	Free water	H_2O
M	+5.2 ± 0.2	Isolated pairs of strongly coupled protons in the c-channel of hydroxylapatite	
^{31}P		**Structural assignment of PO_4^{3-} tetrahedra**	
A	+2.3 ± 0.1	PO_4^{3-} tetrahedra in well-orderd hydroxylapatite	HAp
B	+1.5 ± 0.2	Strongly distorted PO_4^{3-} environment without neighboring OH^-	TCP (TTCP)
C	+3.0 ± 0.2	Distorted PO_4^{3-} tetrahedra with single or paired OH^- groups	O-HAp
D	+5.0 ± 0.2	Very strongly distorted PO_4^{3-} tetrahedra without associated OH^- groups	OAp →TTCP

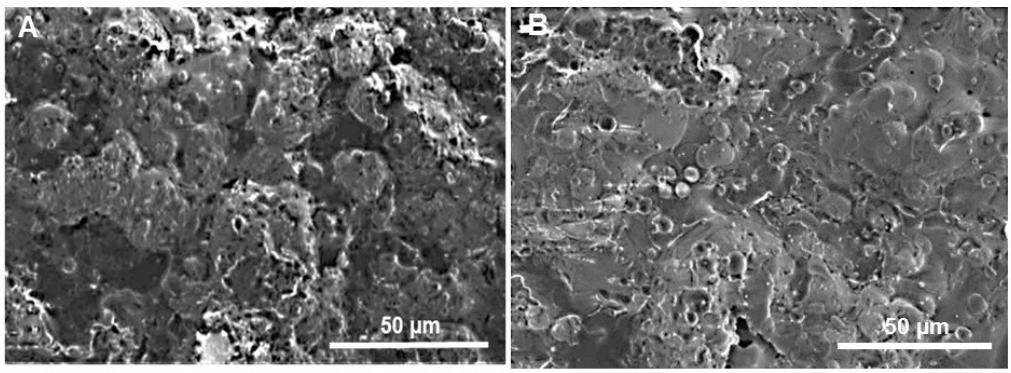

510

511 Figure 1

512

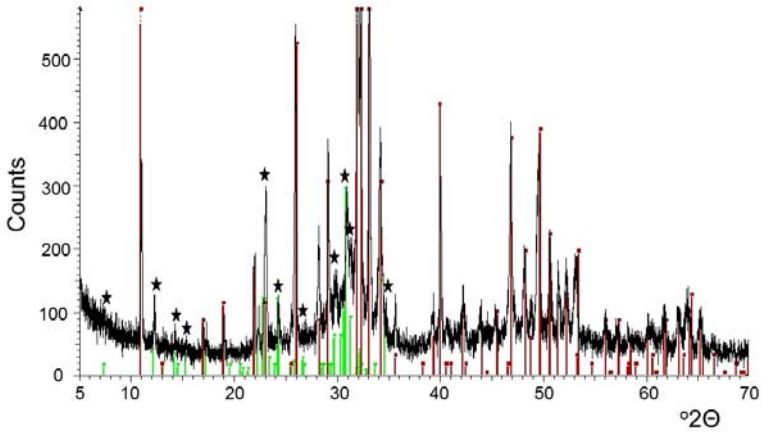

513

514 Figure 2

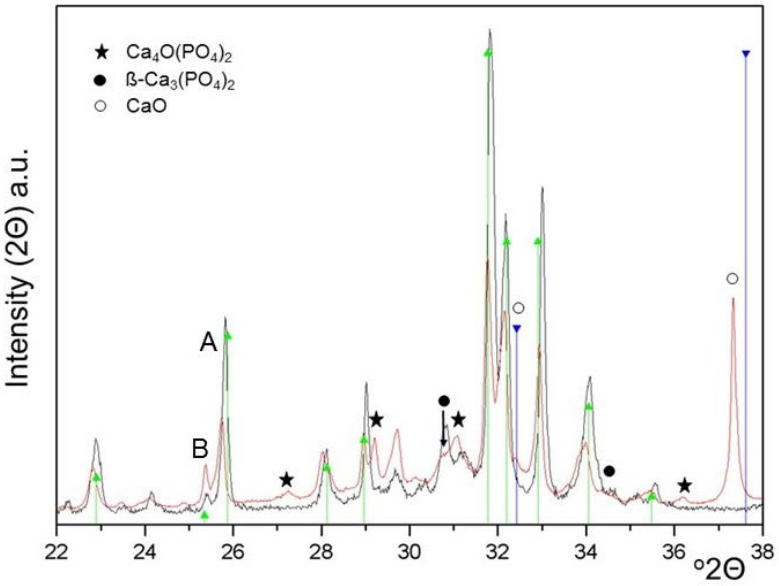

515

516 Figure 3

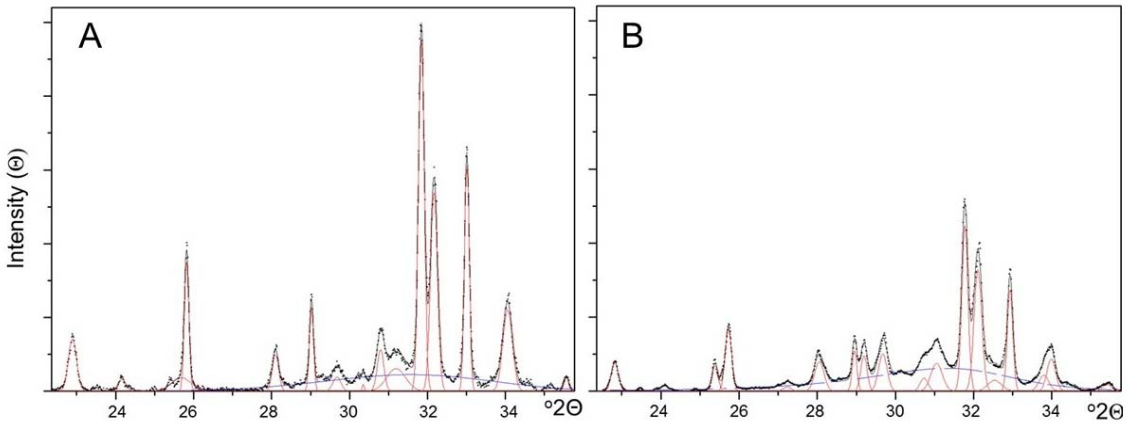

Figure 4

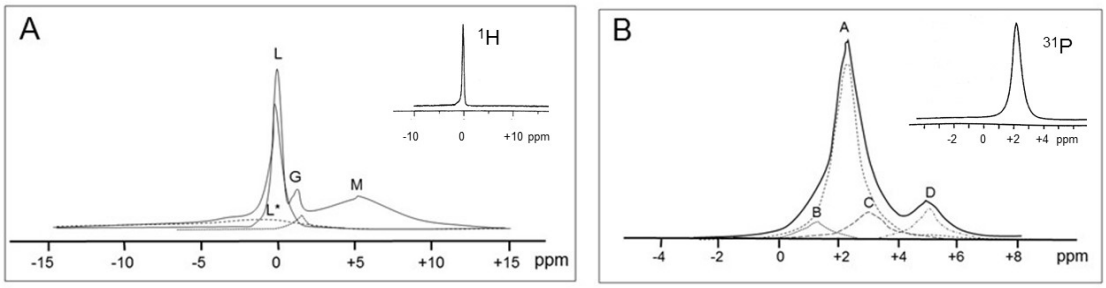

Figure 5